# Energy Management Strategy for Dual IM-PMSM Electric Vehicles

**An-Toan Nguyen [1,4] Binh-Minh Nguyen [2] João Pedro F. Trovão [1,3] Minh C. Ta [1]**

*1) Dept. of Electrical and Computer Engineering, Université de Sherbrooke, Sherbrooke, QC, J1K 2R1, Canada*
*E-mail: An.Toan.Nguyen@USherbrooke.ca, Joao.Trovao@USherbrooke.ca, Cao.Minh.Ta@USherbrooke.ca*
*2) Dept. of Advanced Energy, the University of Tokyo, Tokyo, Japan*
*E-mail: nguyen.binhminh@edu.k.u-tokyo.ac.jp*
*3) Polytechnic of Coimbra, IPC-ISEC and INESC Coimbra, 3030-199 Coimbra, Portugal*
*4) Faculty of Engineering and Technology, Quy Nhon University, Quy Nhon, Binh Dinh, Vietnam*

**ABSTRACT**: This paper proposes a model-based control system to extend the range of dual-motor all-wheel-drive electric vehicles (EVs) across various electric motor (EM) configurations. By analyzing the dynamics of EMs, wheels, and chassis, a cost function is formulated to minimize input power, taking into account driving force distribution and motor current. An optimal strategy for driving force and EM current distribution is developed for real-time implementation on conventional EV electronic control units. Computer simulations demonstrate the effectiveness of this strategy in both constant speed and dynamic driving scenarios.

**KEY WORDS**: Electric vehicle, Dual-motor All-wheel drive, Energy efficiency optimization, Driving force distribution

## 1. INTRODUCTION

Electric Vehicles (EVs) face several challenges including limited range, charging time, battery cost and weight, with range being the primary concern. This has led to extensive research into multi-motor powertrains, particularly the dual-motor all-wheel-drive (DM-AWD) configuration, which utilizes electric motors (EMs) on both the front and rear axles. The DM-AWD setup offers advantages such as the ability to switch between two-wheels and all-wheel drive for improved control, continued operation during motor failures, and optimized torque distribution to reduce energy consumption and enhance drivability. This paper presents an Energy Management Strategy (EMS) developed to achieve energy savings in DM-AWD EVs.

Current torque distribution strategies often rely on simple, rule-based approaches, which lack efficiency and robustness [1]. While some strategies aim to optimize energy distribution, they focus on global dynamics, such as vehicle speed and acceleration, without fully considering the local dynamics of EMs and wheels, including motor speed, current, driving force, and slip ratio [2]. Although an EMS based on transmission efficiency and torque distribution has been proposed, it overlooks the dynamics of EMs and wheel, where slip ratio can lead to significant energy loss, particularly on low-friction surfaces [3].

To address these limitations, this paper proposes a driving force and EM current distribution strategy for minimizing power consumption in DM-AWD EVs. Key contributions include (1) a comprehensive input power model that incorporates the dynamics of motors, wheels, and chassis for both induction motor (IM) and permanent magnet synchronous motor (PMSM) configurations; (2) a framework that links global and local dynamics by integrating vehicle dynamics with wheel dynamics and connecting inner and outer control layers for torque and current distribution; (3) an optimal driving force and EM current distribution strategy that minimizes energy consumption and is suitable for real-time implementation.

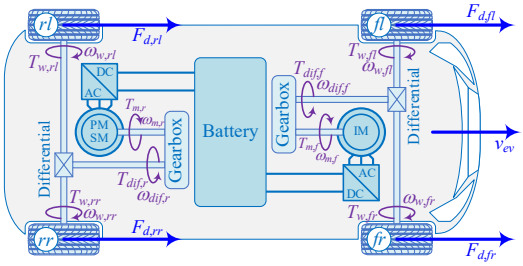


Fig. 1 Modelling of studied vehicle dynamics.

The following sections will present the configuration of the studied vehicle and driving force distribution strategy, followed by an optimal solution for input power minimization. A case study will then validate the proposed strategy, and the conclusion will summarize the results and mention future works.

## 2. CONFIGURATION OF THE STUDIED VEHICLE

The DM-AWD configuration of the studied EV is presented in Fig. 1. The studied EV features two different EMs, with an IM mounted on the front axle and a PMSM mounted on the rear axle. To simplify the presentation, the latter sections of this paper will adopt a unified notation for similar elements on the front and rear axles. The subscript "$i$" will denote either the front "$f$" or rear "$r$" axle, while the subscript "$j$" will represent the left "$l$" or right "$r$" wheel of each axle. Table 1 summarizes the key nomenclature used to describe the studied EV model. Since this paper focuses on longitudinal motion, the left and right driving forces at each drivetrain are assumed to be equal, i.e., $F_{d,il} = F_{d,ir} = 0.5F_{d,i}$ and $\omega_{w,il} = \omega_{w,ir} = \omega_{w,i}$.

## 3. PROPOSED DRIVING FORCE DISTRIBUTION STRATEGY

### 3.1. Driving Force Distribution Approach

Fig. 2 illustrates the driving force and EM current distribution diagram, where the proposed EMS calculates $F^*_{d,f}$ and $F^*_{d,r}$ based on the ratio $k_f$, $F^*_{d,f} = k_f F^*_{tot}$ and $F^*_{d,r} = (1-k_f)F^*_{tot}$. The calculated forces $F^*_{d,f}$ and $F^*_{d,r}$ are distributed to the front and rear powertrains as torques $T^*_{m,f}$ and $T^*_{m,r}$ (1). Each powertrain includes a shared battery, an inverter, and an EM equipped with current controllers that track reference values $i^*_{d_{IM}}$ and $i^*_{d_{PM}}$. A detailed description of the control structure can be found in [4].

$$\begin{cases} T_{m_{IM}} \simeq \dfrac{r_w}{G_f} F_{d,f} = \dfrac{r_w}{G_f} k_f F_{tot} \\ T_{m_{PM}} \simeq \dfrac{r_w}{G_r} F_{d,r} = \dfrac{r_w}{G_r} (1-k_f) F_{tot} \end{cases} \quad (1)$$

where $0 \le k_f \le 1$. For $k_f = 1$, the front IM would exclusively supply $F_{tot}$ to the EV. Conversely, when $k_f = 0$, the rear PMSM would be solely responsible for providing $F_{tot}$.

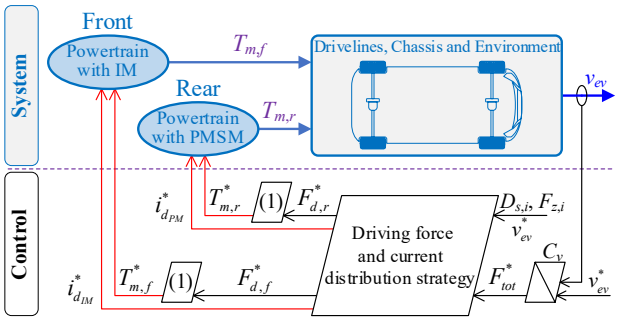


Fig. 2 Driving force and EM current distribution scheme for DM-AWD EVs.

### 3.2. Energy Optimization Problem

The dynamic models of IM and PMSM structured have been previously presented by our research [4]. To maintain conciseness, this paper focuses on describing the power model based on the variables of the longitudinal motion model.

Output power, copper loss, and iron loss of IM [5]

$$P_{m_{IM}} = \omega_{m,f} T_{m,f} \tag{2}$$

$$P_{cu_{IM}} = R_{s_{IM}}\left(i_{d_{IM}}^2 + i_{q_{IM}}^2\right) + R_{r_{IM}} \frac{L_{m_{IM}}^2}{L_{r_{IM}}^2} i_{q_{IM}}^2 \tag{3}$$

$$P_{fe_{IM}} = \frac{\omega_{e_{IM}}^2 L_{m_{IM}}^2}{R_{m_{IM}}}\left(i_{d_{IM}}^2 + \frac{L_{lr_{IM}}^2}{L_{r_{IM}}^2} i_{q_{IM}}^2\right) \tag{4}$$

Output power, copper loss, and iron loss of PMSM [6]

$$P_{m_{PM}} = \omega_{m,r} T_{m,r} \tag{5}$$

$$P_{cu_{PM}} = R_{s_{PM}}\left(i_{d_{PM}}^2 + i_{q_{PM}}^2\right) \tag{6}$$

$$P_{fe_{PM}} = K_{fe_{PM}} \omega_{e_{PM}}^{\gamma} \left[\left(\psi_{r_{PM}} + L_{sd_{PM}} i_{d_{PM}}\right)^2 + L_{sq_{PM}}^2 i_{q_{PM}}^2\right] \tag{7}$$

where $\gamma = 1.5 \sim 1.6$ and $K_{fe_{PM}}$ the iron loss coefficient of PMSM.

Input power model based on (2)~(7)

$$P_{tot} = P_{m_{IM}} + P_{m_{PM}} + P_{cu_{IM}} + P_{cu_{PM}} + P_{fe_{IM}} + P_{fe_{PM}} \tag{8}$$

By applying the mathematical transformations developed by our research group [7] to (2)~(7), the power model of the motors can be expressed in terms of the variables of the longitudinal motion model as follows for IM and PMSM.

#### 3.2.1. Power Model of IM

$$\tilde{P}_{m_{IM}} = v_{ev}\left(k_f F_{tot} + \frac{k_f^2 F_{tot}^2}{D_{s,f} F_{z,f}}\right) \tag{9}$$

$$\tilde{P}_{cu_{IM}} = R_{s_{IM}}\left(i_{d_{IM}}^2 + \frac{k_{IM}^2 k_f^2 F_{tot}^2}{i_{d_{IM}}^2}\right) + \frac{R_{r_{IM}} L_{m_{IM}}^2 k_{IM}^2 k_f^2 F_{tot}^2}{L_{r_{IM}}^2 i_{d_{IM}}^2} \tag{10}$$

$$\tilde{P}_{fe_{IM}} = \frac{L_{m_{IM}}^2}{R_{m_{IM}}}\left\{\begin{array}{l}\left(i_{d_{IM}}^2 + \dfrac{L_{lr_{IM}}^2 k_{IM}^2 k_f^2 F_{tot}^2}{L_{r_{IM}}^2 i_{d_{IM}}^2}\right) \\ \cdot\left(\dfrac{p_{n_{IM}} G_f v_{ev}}{r_w} + \dfrac{R_{r_{IM}} k_{IM} k_f F_{tot}}{L_{r_{IM}} i_{d_{IM}}^2}\right)^2\end{array}\right\} \tag{11}$$

where

$$k_{IM} = \frac{r_w L_{r_{IM}}}{1.5 p_{n_{IM}} L_{m_{IM}}^2 G_f} \tag{12}$$

Voltage and current constraints of IM:

$$\left\{\begin{array}{l} L_{s_{IM}}^2\left(\dfrac{p_{n_{IM}} G_f v_{ev}}{r_w} + \dfrac{R_{r_{IM}} k_{IM} k_f F_{tot}}{L_{r_{IM}} i_{d_{IM}}^2}\right) \\ \cdot\left[i_{d_{IM}}^2 + \dfrac{k_{IM}^2 k_f^2 F_{tot}^2}{i_{d_{IM}}^2}\cdot\left(1 - \dfrac{L_{m_{IM}}^2}{L_{s_{IM}} L_{r_{IM}}}\right)^2\right]\end{array}\right\} \le \frac{u_{bat}^2}{3} \tag{13}$$

$$i_{d_{IM}}^2 + \frac{k_{IM}^2 k_f^2 F_{tot}^2}{i_{d_{IM}}^2} \le I_{max_{IM}}^2 \tag{14}$$

$$0 < i_{d_{IM}} \le I_{dn_{IM}} \tag{15}$$

Table 1 Nomenclature

| Symbol | Description |
|---|---|
| | ***Mechanical*** |
| $D_{s,i}$ | Driving stiffness coefficient of the wheels at each drivetrain |
| $F_{d,i}$ | Driving force on each drivetrain |
| $F_{d,ij}$ | Driving force of each wheel |
| $F_{tot}$ | Total environmental resistance force acting on the vehicle |
| $F_{z,i}$ | Vertical force acting at the front or rear wheels |
| $G_i$ | Gear ratio on each drivetrain |
| $K_{hs,ij}$ | Stiffness coefficient of each half-shaft |
| $k_f$ | Driving force distribution ratio for the front wheels |
| $r_w$ | Wheel radius |
| $T_{m,i}$ | Torque of each motor |
| $T_{trac,ij}$ | Torque of each wheel |
| $v_{ev}$ | Longitudinal velocity of the vehicle body |
| $\omega_{m,i}$ | Mechanical angular speeds of each motor |
| $\omega_{w,i}$ | Angular speed of the front or rear wheels |
| $\omega_{w,ij}$ | Angular speed of each wheel |
| | **Electrical** |
| $i_{d_{IM}}, i_{q_{IM}}$ | *d-q* axes stator currents of IM |
| $i_{d_{PM}}, i_{q_{PM}}$ | *d-q* axes stator currents of PMSM |
| $L_{sd_{PM}}, L_{sq_{PM}}$ | *d-q* axes stator inductances of PMSM |
| $L_{m_{IM}}, L_{lr_{IM}}$ | Magnetizing and rotor leakage inductances of IM |
| $L_{r_{IM}}$ | Rotor inductances of IM |
| $p_{n_{IM}}, p_{n_{PM}}$ | Number of pole pairs of IM and PMSM |
| $u_{bat}$ | Battery voltage |
| $R_{m_{IM}}$ | Magnetizing resistance of IM |
| $R_{r_{IM}}$ | Rotor resistance of IM |
| $R_{s_{IM}}, R_{s_{PM}}$ | Stator resistance of IM and PMSM |
| $\psi_{r_{PM}}$ | Permanent magnet rotor flux linkage of PMSM |
| $\omega_{e_{IM}}, \omega_{e_{PM}}$ | Synchronous angular speed of IM and PMSM |

#### 3.2.2. Power Model of PMSM

$$\tilde{P}_{m_{PM}} = v_{ev}\left[(1-k_f)F_{tot} + \frac{(1-k_f)^2 F_{tot}^2}{D_{s,r} F_{z,r}}\right] \tag{16}$$

$$\tilde{P}_{cu_{PM}} = R_{s_{PM}}\left[i_{d_{PM}}^2 + \frac{k_{PM}^2 (1-k_f)^2 F_{tot}^2}{\psi_{r_{PM}}^2}\right] \tag{17}$$

$$\tilde{P}_{fe_{PM}} = K_{fe_{PM}}\left(\frac{p_{n_{PM}} G_r v_{ev}}{r_w}\right)^{\gamma} \cdot\left\{\left(\psi_{r_{PM}} + L_{d_{PM}} i_{d_{PM}}\right)^2 + \frac{L_{q_{PM}}^2 k_{PM}^2 (1-k_f)^2 F_{tot}^2}{\psi_{r_{PM}}^2}\right\} \tag{18}$$

where

$$k_{PM} = \frac{r_w}{1.5 p_{n_{PM}} G_r} \tag{19}$$

Voltage and current constraints of PMSM:

$$\left(\frac{p_{n_{PM}} G_r v_{ev}}{r_w}\right)^2 \left\{\begin{array}{l}\left(L_{d_{PM}} i_{d_{PM}} + \psi_{r_{PM}}\right)^2 \\ + \dfrac{L_{q_{PM}}^2 k_{PM}^2 (1-k_f)^2 F_{tot}^2}{\psi_{r_{PM}}^2}\end{array}\right\} \le \frac{u_{bat}^2}{3} \tag{20}$$

$$i_{d_{PM}}^2 + \frac{k_{PM}^2 (1-k_f)^2 F_{tot}^2}{\psi_{r_{PM}}^2} \le I_{max_{PM}}^2 \tag{21}$$

$$-\frac{\psi_{r_{PM}}}{L_{d_{PM}}} \le i_{d_{PM}} \le 0 \tag{22}$$

#### 3.2.3. Optimal solution for input power minimization

The total input power to the EV's motors is the sum of the powers and losses calculated above

$$\begin{aligned}\tilde{P}_{tot} &= \tilde{P}_{m_{IM}} + \tilde{P}_{m_{PM}} + \tilde{P}_{cu_{IM}} + \tilde{P}_{cu_{PM}} + \tilde{P}_{fe_{IM}} + \tilde{P}_{fe_{PM}} \\ &= \Im_1 \frac{k_f^4}{i_{d_{IM}}^6} + \Im_2 \frac{k_f^3}{i_{d_{IM}}^4} + \Im_3 \frac{k_f^2}{i_{d_{IM}}^2} + \Im_4 k_f^2 - \Im_5 k_f \\ &\quad + \Im_6 i_{d_{IM}}^2 + \Im_7 i_{d_{PM}}^2 + \Im_8 i_{d_{PM}} + \Im_9\end{aligned} \tag{23}$$

Fig. 3 e-Commander Platform at e-TESC Lab.

where $\Im_1$~$\Im_9$ are coefficients containing motor parameters and variables $v_x$, $F_{tot}$, $D_{s,i}$ and $F_{z,i}$.

Given the relative insignificance of $k_f$=0~1 to $i_{d_{IM}}$, terms such as $\frac{k_f^4}{i_{d_{IM}}^6}$ and $\frac{k_f^3}{i_{d_{IM}}^4}$ in (23) are negligible. As a result, the total input power model can be simplified to a reduced second-order polynomial by eliminating higher-order components

$$\tilde{P}_{tot} \simeq \left(\frac{\Im_3}{i_{d_{IM}}^2} + \Im_4\right) k_f^2 - \Im_5 k_f + \Im_6 i_{d_{IM}}^2 + \Im_7 i_{d_{PM}}^2 + \Im_8 i_{d_{PM}} + \Im_9 \tag{24}$$

For a given $v_{ev}$, numerous sets of $(k_f, i_{d_{IM}}, i_{d_{PM}})$ values can produce the desired $F_{tot}$. However, the optimal set $(k_{f_{opt}}, i_{d_{opt,IM}}, i_{d_{opt,PM}})$ minimizes $\tilde{P}_{tot}$ for a given $F_{tot}$ and $v_{ev}$, subject to constraints on $k_f$, voltages, and currents

$$\min_{\{k_f, i_{d_{IM}}, i_{d_{PM}}\}} \tilde{P}_{tot} \quad \text{subject to } 0 \le k_f \le 1, \text{(13)~(15), (20)~(22)} \tag{25}$$

Since the input power minimization problem is an optimization problem under inequality constraints, the Kuhn-Tucker theorem [8] can be applied to calculate the optimal values of $(k_f, i_{d_{IM}}, i_{d_{PM}})$. Regions in optimal values space are then defined such that

$$U_k = \{k_f | 0 \le k_f \le 1\} \tag{26}$$
$$U_{v_{IM}} = \{i_{d_{IM}} | \text{Eq. (13)}\} \tag{27}$$
$$U_{c1_{IM}} = \{i_{d_{IM}} | \text{Eq. (14)}\} \tag{28}$$
$$U_{c2_{IM}} = \{i_{d_{IM}} | \text{Eq. (15)}\} \tag{29}$$
$$U_{v_{PM}} = \{i_{d_{PM}} | \text{Eq. (20)}\} \tag{30}$$
$$U_{c1_{PM}} = \{i_{d_{PM}} | \text{Eq. (21)}\} \tag{31}$$
$$U_{c2_{PM}} = \{i_{d_{PM}} | \text{Eq. (22)}\} \tag{32}$$

Observe that the boundaries of optimal values space contain regular points [8]. The minimum point within the interior region is identified under the following conditions

$$\left.\frac{\partial \tilde{P}_{tot}}{\partial k_f}\right|_{v_{ev}, F_{tot}, D_{s,i}, F_{z,i}} = 0 \tag{33}$$
$$\left.\frac{\partial \tilde{P}_{tot}}{\partial i_{d_{IM}}}\right|_{v_{ev}, F_{tot}, D_{s,i}, F_{z,i}} = 0 \tag{34}$$
$$\left.\frac{\partial \tilde{P}_{tot}}{\partial i_{d_{PM}}}\right|_{v_{ev}, F_{tot}, D_{s,i}, F_{z,i}} = 0 \tag{35}$$

Using (24), condition (33)~(35) is satisfied when

$$\frac{2\Im_3 k_f}{i_{d_{IM}}^2} + 2\Im_4 k_f - \Im_5 = 0 \tag{36}$$
$$-\frac{\Im_3 k_f^2}{i_{d_{IM}}^2} + \Im_6 i_{d_{IM}} = 0 \tag{37}$$
$$2 i_{d_{PM}} \Im_7 + \Im_8 = 0 \tag{38}$$

By solving the set of equations (36)~(38), the optimal values of $(k_f, i_{d_{IM}}, i_{d_{PM}})$ are determined to minimize $\tilde{P}_{tot}$. Solving for $i_{d_{opt,IM}}$ involves solving a fourth-degree equation, which yields four potential solutions. However, considering the non-negativity constraint on $i_{d_{IM}}$, the solution provided by $i_{d_{opt,IM}}$ (39) is selected. Substituting this value of $i_{d_{opt,IM}}$ into (37) yields the corresponding values of $k_{f_{opt}}$ (39). From (38), the value of $i_{d_{opt,PM}}$ is obtained as given in (39). Consequently, the total power minimization condition for the studied EV is given by

$$\begin{cases} i_{d_{opt,IM}} \simeq \sqrt[4]{\dfrac{0.25\Im_3\Im_5^2}{\Im_4^2\Im_6}} \\ i_{d_{opt,PM}} = -\dfrac{0.5\Im_8}{\Im_7} \\ k_{f_{opt}} = \dfrac{0.5\Im_5 i_{d_{IM}}^2}{\Im_3 + \Im_4 i_{d_{IM}}^2} \end{cases} \tag{39}$$

If the values determined in (39) violate any of the boundary conditions (26)~(32), the corresponding variable will be recalculated according to the violated boundary condition.

## 4. SIMULATION FOR COMPARATIVE EVALUATION

### 4.1. Simulation Setup

The proposed driving force distribution is validated in the MATLAB/Simulink® environment to evaluate the performance of the strategy for DM-AWD EVs. The parameters of the studied vehicle are based on the e-Commander platform at e-TESC Lab (Fig. 3), and its modelling is described in [4]. The reference velocity of the EV follows the driving cycle WLTC class 2 (WLTC2) with road friction coefficient $\mu = 0.87$.

### 4.2. Results and Discussion

Fig. 4 shows that the vehicle closely follows the velocity profile specified by WLTC2. The optimal distribution value as shown in (39), is employed to distribute the driving force and *d*-axis current for EMs in Fig. 2. This result confirms the effectiveness of the proposed strategy in allocating appropriate torque to both motors.

Fig. 4 also describes the optimal driving force distribution ratio $k_{f_{opt}}$ of the proposed EMS with WLTC2. The magnitude and variation of this ratio are primarily influenced by vehicle acceleration. During acceleration, the ratio typically exceeds 0.5, indicating that a greater proportion of the driving force is allocated to the IM. Conversely, during deceleration, the ratio tends to fall

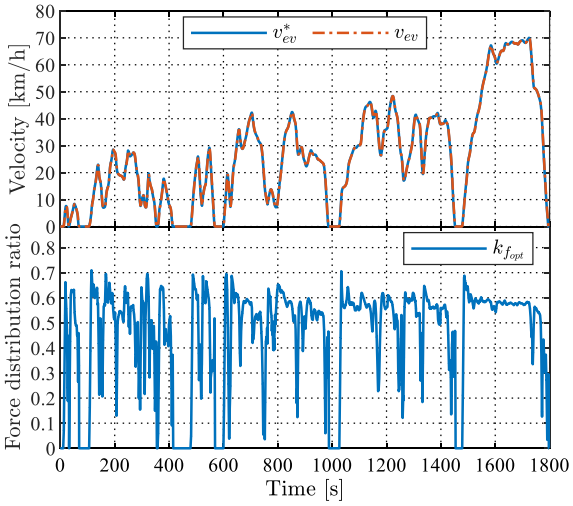


Fig. 4 Velocity responses and optimal driving force distribution ratio of the proposed EMS with WLTC2.

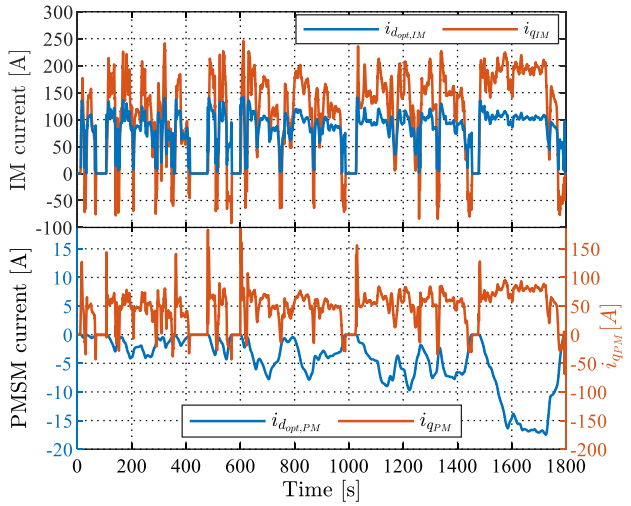


Fig. 5 *d-q* axes stator currents of EMs with WLTC2.

below 0.5, indicating that a higher proportion of the driving force is allocated to the PMSM.

Fig. 5 illustrates the *dq*-axes stator current responses of the IM and PMSM. The reference *d*-axis currents correspond to the optimal values calculated using (39). It is clearly shown that their values vary according to working conditions to ensure optimal force distribution, thus minimizing energy consumption.

The proposed strategy relies on approximations to obtain the input power of EMs $\tilde{P}_{tot}$. To validate the accuracy of these approximations, Fig. 6 compares $\tilde{P}_{tot}$ (24) with the power consumption $P_{tot}$ (8) under WLTC2 conditions for a specific value of $k_{f_{opt}}$. While minor discrepancies are observed, particularly in the high-speed region, $P_{tot}$ consistently exceeds $\tilde{P}_{tot}$. This confirms that reducing $\tilde{P}_{tot}$ through the proposed strategy will lead to a corresponding reduction in actual power consumption, aligning with the paper's objectives.

Fig. 6 further demonstrates the effectiveness of the proposed strategy in reducing energy consumption. The total power loss of the EMs using the proposed strategy is consistently lower than that of the method using a constant $k_f$. This reduction is particularly significant in the high-speed region. These results highlight the effectiveness of the proposed strategy in minimizing power consumption, despite its reliance on approximations and simple calculations.

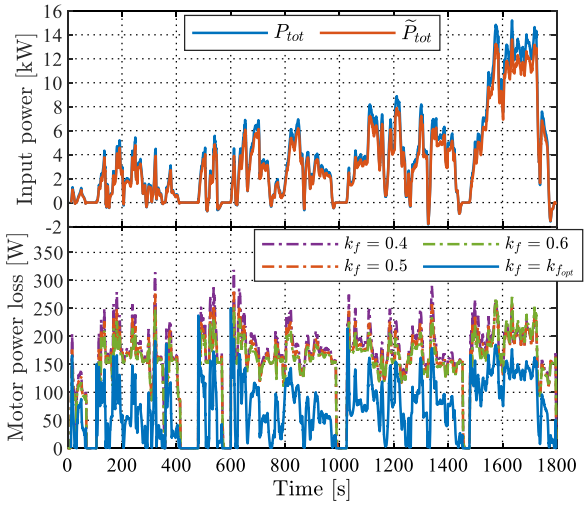


Fig. 6 Total power input and total power loss of EMs with WLTC2.

## 5. CONCLUSIONS

This paper presents a model-based range extension control strategy for DM-AWD EVs that optimizes driving force distribution between front and rear wheels. By incorporating the dynamics of motors, wheels, and chassis, an input power model is developed for dual IM-PMSM EVs and used as a cost function to minimize energy consumption. A simple yet effective strategy for optimizing driving force distribution is proposed. Simulation results confirm the effectiveness of the strategy in extending the cruising range of DM-AWD EVs. Future work will focus on validation using the e-Commander platform at the e-TESC Lab.

## ACKNOWLEDGMENT

This research was supported by the Startup grant No. 4124-05 from the Faculty of Engineering of University of Sherbrooke, Canada and by the Grant No. RGPIN-2024-06787 from the Natural Sciences and Engineering Research Council of Canada.

This work is also supported in part by the Japan Grants-in-Aid for Scientific Research No. 22K14283, and the Nagamori Research Grant.

## REFERENCES

(1) De Pinto S., Camocardi P., Sorniotti A., Gruber P., Perlo P., Viotto F., "Torque-Fill Control and Energy Management for a Four-Wheel-Drive Electric Vehicle Layout With Two-Speed Transmissions," *IEEE Trans. Ind. Appl.*, vol. 53, no 1, pp.447-458, 2017.

(2) Nguyen C.T.P., Nguyễn B.-H., Trovão J.P.F., Ta M.C., "Torque Distribution Optimization for a Dual-Motor Electric Vehicle Using Adaptive Network-Based Fuzzy Inference System," *IEEE Trans. Energy Convers.*, vol. 38, no. 4, pp. 2784-2795, 2023.

(3) Vo-Duy T., Doan T.-M., Nguyễn B.-H., Trovão J.P.F., "Optimal Energy Management System of Dual-motor Electric Vehicles with Longitudinal Dynamic Characteristic Consideration," *IEEE Trans. Veh. Technol.*, pp. 1-13, 2023.

(4) Nguyen A.-T., Nguyen B.-M., Trovão J.P.F., Ta M.C., "Modelling and Control of Dual-Motor All-Wheel Drive Electric Vehicles using Energetic Macroscopic Representation," *In: Proceedings of the Canadian Society for Mechanical Engineering International Congress (CSME - CFD-SC2023)*, pp. 1-6, 2023.

(5) Nam K.H., *AC Motor Control and Electrical Vehicle Applications*, CRC Press; 2018.

(6) Krause P., Wasynczuk O., Sudhoff S., Pekarek S., eds. *Analysis of Electric Machinery and Drive Systems*, Wiley, 2013.

(7) Nguyen B.-M., Trovão J.P.F., Ta M.C., "Double-Layer Energy Management for Multi-Motor Electric Vehicles," IEEE Trans. Veh. Technol., vol. 72, no. 7, pp. 8623-8635, 2023.

(8) Luenberger D.G., Ye Y., *Linear and Nonlinear Programming*, Springer International Publishing; 2016.